Chirico, G., Barakos, G. N. and Brown, N. (2018) Acoustic Assessment of Twin-engined Turboprop Layout. In: 6th European Conference on Computational Mechanics (ECCM 6) 7th European Conference on Computational Fluid Dynamics (ECFD 7), Glasgow, UK, 11-15 Jun 2018.

There may be differences between this version and the published version. You are advised to consult the publisher's version if you wish to cite from it.

Deposited on: 19 March 2018

ACOUSTIC ASSESSMENT OF TWIN-ENGINED TURBOPROP LAYOUTS

GIULIA CHIRICO[1], GEORGE N. BARAKOS[2] and NICHOLAS BOWN[3]

[1] CFD Laboratory
University of Glasgow, G12 8QQ, UK
g.chirico.1@research.gla.ac.uk

[2] CFD Laboratory
University of Glasgow, G12 8QQ, UK
George.Barakos@glasgow.ac.uk

[3] Dowty Propellers
Anson Business Park, Cheltenham Road East, Gloucester, GL2 9QN, UK
Nicholas.Bown@dowty.com

Key words: turboprop acoustics, CFD, installation effects, cabin noise

Abstract. Turboprop aircraft are fuel efficient on short and medium range flights but their noise emissions are higher than future aviation targets and standards. The flow solver HMB3 is used here to analyse the sound field of a full-scale twin-engined turboprop to assess the quietest installation layout. The eight-bladed IMPACTA propeller is used in this research and cruise operating conditions are assumed. Overall sound pressure levels on the fuselage exterior surface are evaluated directly from the CFD solution. Cabin noise is also estimated through experimentally obtained transfer functions.

The employed method showed marked differences among the various installation options, capturing the complex acoustic field generated by the propellers and underlying the need of simulating the whole airframe for accurate predictions. Synchrophasing on a co-rotating propeller aircraft appears to be acoustically beneficial, especially regarding the interior sound, but the noise reduction provided by a counter-rotating layout with inboard-down direction is larger. The inboard-up rotational direction shows louder sound because of inflow conditions and the occurrence of constructive acoustic interferences between the sound of the two propellers and those generated by the airframe.

1 INTRODUCTION

1.1 Motivation and Objectives

Up to 95% of the total air traffic on European routes are short and medium range flights. Having a considerably higher propulsive efficiency in comparison to a similar capacity jet aircraft, propeller-driven aircraft are the best option for reducing fuel burnt. However, current

turboprops still show an interior noise around 25 dB louder, on average, than a turbofan aircraft and, because of the several tone components forming the propeller sound spectra, they are perceived by passengers as more annoying. In addition, future environmental certifications will also require a cut in the aircraft acoustic emissions[1, 2]. Therefore, in line with the challenge of improving turboprops acoustics (without a high performance penalty) this work compares various propeller installation layouts aiming to find the quietest option. Co-rotating and counter-rotating propellers are considered: the first layout usually preferred for civil aircraft because of lower maintenance costs and easier logistics, the latter encountered in military aircraft because of the natural balance of roll and yaw moments and of the P-factor. Synchrophasing is also investigated for the co-rotating option as it had previously proven effective in reducing both vibration and noise levels. The objective of the present research is not to estimate the absolute noise levels of each propeller installation layout, but to perform a relative study to assess if one configuration is acoustically advantageous with respect to the others.

1.2   Past and Current Work

Installed propellers were initially studied in the eighties and nineties when high oil prices made them an attractive alternative to the wider employed turbojets. Both aerodynamics and acoustics were investigated, linked to the aircraft sale and usage costs. Major projects were carried out, experimentally and numerically, in the USA and Europe. Among these we recall the PTA project[3, 4, 5, 6, 7, 8] of NASA, GEMINI II[9, 10, 11] and APIAN[12, 13] of the European Commission and the research activities of FAA and SAAB[14, 15, 16, 17, 18, 19]. Relevant findings for this research are: *(i)* propeller and airframe are subjected to an unsteady mutual interaction, so 3D time marching simulations are needed to accurately capture the phenomena[9, 10, 11, 12, 13]; *(ii)* to acceptably predict noise levels, airframe reflections, scattering and boundary layer refraction need to be accounted for, and thus a direct noise computation, as it naturally accounts for these non-linear effects, can be a "viable and reliable" near-field noise technique[8]; *(iii)* the cabin noise is mainly affected by the first three propeller harmonics[19]. Nowadays, CFD techniques are often employed to study the near-field acoustics of installed propellers (see e.g. [20, 21, 22, 23]), analysing a propeller-engine-wing combination.

Studies on synchrophasing also started in the eighties. Analytical and experimental investigations using monopole/dipole sources and a cylindrical shell[24, 25] showed that: *(i)* the propeller phase angles do not affect so much the external pressure field but alter the internal cabin pressure that is directly coupled with structural vibration modes of the fuselage; *(ii)* the majority of the acoustic energy gets into the fuselage over a length of one shell diameter, going in and out in localized areas with positions strongly dependent on the propeller phase shift. Results of an analytical technique combining propellers signatures in the frequency domain applied to flight-test data proved that synchrophasing is able to lower the average interior sound levels by up to 8 dB in four-engined aircraft and by 1.5 dB in twin-engined[26, 27]. The optimum synchrophase angle is found, in the above works, to depend on cabin location, sound frequency and fuselage layout, and, in recent research[28], to also change with flight and environmental conditions. Hence, the choice of the synchrophase angle is a compromise and configuration-dependent, and ideally the synchrophaser should be adaptive (for investigations on adaptive synchrophasing

controllers see for example [29, 30, 31, 32, 33, 34]). Nevertheless usually the synchrophase angles are set a priori via a preliminary optimisation study which is still performed using the propeller signature theory with experimental data[35, 36], assuming that the contributions of the propellers are combined in a linear way. This appears a reasonable assumption but it is not well proven.

This work, in contrast, considers a whole twin-engined turboprop aircraft and uses CFD to investigate the complex acoustic near-field that is generated by the direct sound fields of the two propellers and the interactions between each other and with the airframe. The characteristics of the external pressure field, for the different propeller installation layouts considered, are analysed directly from the CFD solutions aiming to identify the noise source mechanisms that develop in each case. The interior noise is also evaluated, via transfer functions, to assess if, and how, the various options modify the cabin sound perceived by passengers. In this way, the overall acoustics of the different installation strategies is evaluated.

2 COMPUTATIONAL METHODS

2.1 The CFD Solver HMB3

The computations were performed with the in-house parallel CFD solver Helicopter Multi Block (HMB3)[37, 38, 39] of the University of Glasgow. HMB3 solves the 3D Navier-Stokes equations in dimensionless integral form using the Arbitrary Lagrangian Eulerian formulation for time-dependent domains with moving boundaries, discretised via a cell-centered finite volume approach on a curvilinear co-ordinate system. Convective fluxes are treated with Osher's upwind scheme[40] and the viscous stress tensor is approximated using the Boussinesq hypothesis[41] or an explicit algebraic Reynolds stress model[42]. Several turbulence models, of the URANS and hybrid LES/URANS families, are implemented in the solver. The MUSCL variable extrapolation method[43] is employed, in combination with the van Albada limiter[44], to provide second-order accuracy and avoid spurious oscillations across shock waves. The temporal integration is performed with an implicit dual-time method and the linear system is solved using the generalized conjugate gradient method with a BILU[45] factorization as a pre-conditioner.

Solver Validation HMB3 showed accurate predictions for the flow around the propeller blades, the aerodynamic phenomena due to the propeller-airframe interaction and the acoustic near-field dominant tones. Comparison of the HMB3 numerical results against experimental data are presented in [46] and [47] for an isolated and an installed configurations, respectively.

2.2 Noise Estimation Approach

External Noise The near-field noise is directly estimated from the CFD solution. The time history of the pressure field $p(\mathbf{x}, t)$ is extracted from the flow-field at different time steps or recorded by numerical probes at points of interest in the case of unsteady computations.

The Overall Sound Pressure Level (OSPL) and the Sound Pressure Level (SPL) as function of

the sound frequency are computed as follows:

$$\begin{cases} OSPL = 10\log_{10}\left(\frac{p'_{rms}{}^2}{p_{\text{ref}}{}^2}\right) \text{dB}, \\ SPL(f) = 10\log_{10}\left(\frac{PSD(p')}{p_{ref}{}^2}\right) \text{dB}, \end{cases} \tag{1}$$

where $p'(\mathbf{x}, t)$ is the unsteady pressure field, rms stands for root mean square, PSD is the power spectral density and p_{ref} is the acoustic reference pressure which is equal to $2 \cdot 10^{-5}$ Pa.

Internal Noise The interior noise is evaluated via experimentally obtained Transfer Functions[48] (TF) that take into account the aircraft structural response without the need of a computationally expensive structural model (a stronger coupling between aeroacoustics and structural vibrations is beyond the scope of the analysis at this stage). Data recorded from the numerical probes on the aircraft fuselage are used as input. The passenger considered in this analysis is located on the starboard side of the airplane, slightly ahead of the propeller rotational plane on the second seat from the window, which is one of the areas with higher noise levels in the case of standard co-rotating layouts. For a more detailed description of the TF determination and their application please refer to [47]. It is noted that the TF are used to compare the interior acoustics of the different propeller designs or installation layouts, without any intention to estimate absolute noise levels.

## 3   NUMERICAL SETUP

3.1   Test Cases

The propeller employed in this study is the Baseline design of the eight-bladed IMPACTA propeller[47]. It is a new-generation propeller, designed with an extremely low activity factor and operating at high blade loading conditions. Geometric parameters and flight cruise conditions are reported in Table 1. In this work a cruise flight is considered, being usually the longer segment of the aircraft route where propellers are the major noise source. Results can differ in climb because of the different propeller operating conditions.
A twin-engined turboprop with a generic shape representative of a 70-80 passenger standard commercial high-wing design, similar to the ATR72 or the Bombardier Dash 8, was considered (see Figure 1(a)). No geometry simplifications are introduced apart from the lack of the tail that is not altering the cabin noise.

Table 1: IMPACTA Baseline propeller parameters and nominal cruise operating conditions.

Radius R	2.21 m	Free-stream Mach number M_∞	0.5
Root chord c	0.213 m	Thrust line incidence	-2 deg
Pitch angle (0.7R)	$\sim 51°$	Helical Mach number (0.95R)	0.789
Angular velocity	~ 850 RPM	Tip Reynolds number Re_{TIP}	1.24e06
Required Thrust	7852 N	Altitude	7620 m

4
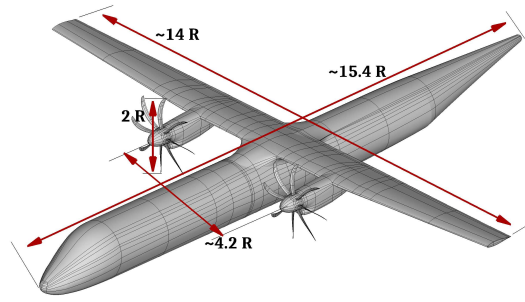
(a) Computational geometry with dimensions as function of the propeller radius R.
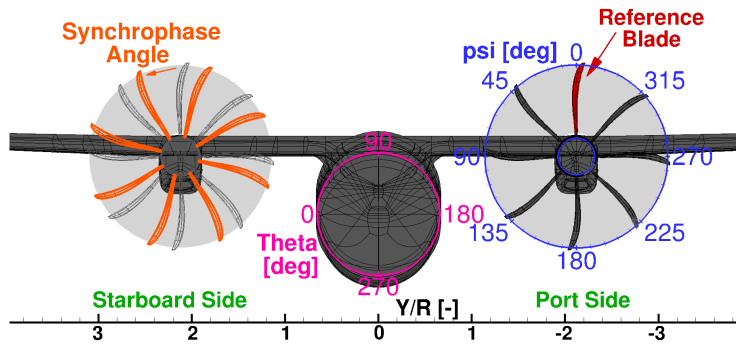
(b) Frontal view: definition of *(i)* synchrophase angle (starboard blades at the reference position, i.e. $\psi_s = 0$ deg, shown in grey, blades shifted by a positive synchrophased angle in orange), *(ii)* fuselage azimuthal coordinate θ, and *(iii)* reference blade azimuthal coordinate ψ_b (increasing with the propeller rotation, regardless of the direction).

Figure 1: Turboprop computational geometry (at the initial instant of the simulation) with system of reference definitions.

The following propeller installation options were analysed[49, 50]:

(a) Co-rotating propellers (CO) - conventional layout for civil aircraft, because of maintenance costs and logistical reasons, with both propellers rotating clockwise as viewed from the rear;

   (a₁) Synchrophased propellers - starboard propeller blades leading those of the port propeller by an angle equal to $\psi_s = 5, 10, 15, 21$ and 30 deg (refer to Figure 1(b));

(b) Counter-rotating top-in propellers (CNTI) - port propeller rotating clockwise and starboard propeller counterclockwise as viewed from the rear, thus both propellers approach the fuselage when moving downwards;

(c) Counter-rotating top-out propellers (CNTO) - port propeller rotating counterclockwise and starboard propeller clockwise as viewed from the rear, thus both propellers approach the fuselage when moving upwards.

The RPM of the two propellers are always assumed to be kept equal, so that the audible vibration that arises if this is not the case is avoided.

Computations were carried out solving the URANS equations with the $k - \omega$ SST turbulence model[51] with a temporal resolution correspondent to 1 degree of propeller azimuth. URANS equations were employed because they are efficient to solve and capture the propeller tonal noise, which is the main contribution to the overall interior noise; no attempt was made at this stage to study the broadband noise content. Numerical probes were included in the simulations to directly record the pressure time history on the aircraft fuselage, in the main propeller region of influence.

3.2 Computational Grids

Multi-block structured grids were built with the ICEM-Hexa™ software. A fully-matched body-fitted mesh of the whole aircraft comprising fuselage, wings and nacelles was generated adopting an "O" grid topology around them. Propellers are inserted using the sliding plane technique[52]. The grids for the different layouts were obtained by selecting the appropriate propellers during the grid assembling process, mirroring the mesh in the case of opposite rotational directions and rotating the starboard propeller drum by the desired angle for synchrophased propellers. A regular background grid extends the airplane mesh until the far-field via the chimera over-set method[53]. Globally, the full grid counts about 170 M cells, of which around 132 M belong to the airplane mesh and around 16.5 million to each propeller. See [49] for a detailed description of the employed grids.

4 DISCUSSION OF THE RESULTS

4.1 Aircraft Exterior Noise

Figure 2 shows the unsteady pressure field around the aircraft at one instant in time, and the OSPL distribution on the aircraft surface, for the co-rotating layout with propellers in phase. As can be seen from the acoustic field visualisations, the employed mesh resolution captures the pressure perturbations generated by the propeller blades and preserves them further downstream, up until the aircraft tail. Noise travelling in the up-stream direction, and emitted from the back of the nacelles, is also observed. The propagation of the acoustic waves, their interaction with the airframe and the interference with other sound waves, are clearly visible in the CFD solutions.

Larger pressure perturbations are seen on the up-stroking blade side because of the higher blade loading at the considered inflow conditions. The pressure perturbation developed by the interaction of the blade tip vortices with the wing leading-edge appears to be significantly larger on the upwards-moving blade side, where the wing is more loaded as affected by the propeller up-wash. Moreover, a constructive interference is observed among the direct sound field generated by the propeller rotation and the acoustic waves emanating by the interactions with the airframe. Therefore, louder noise is expected on the inboard-up propeller side, and this is also evident from the OSPL contours on the aircraft surface. From the fuselage noise distribution it is also noted that the highest sound levels are in proximity to the propeller plane, from about one propeller radius upstream up to the wing trailing edge station.

(a) Transversal plane $1R$ behind the propeller plane.

(b) Longitudinal plane at propeller spinner height.
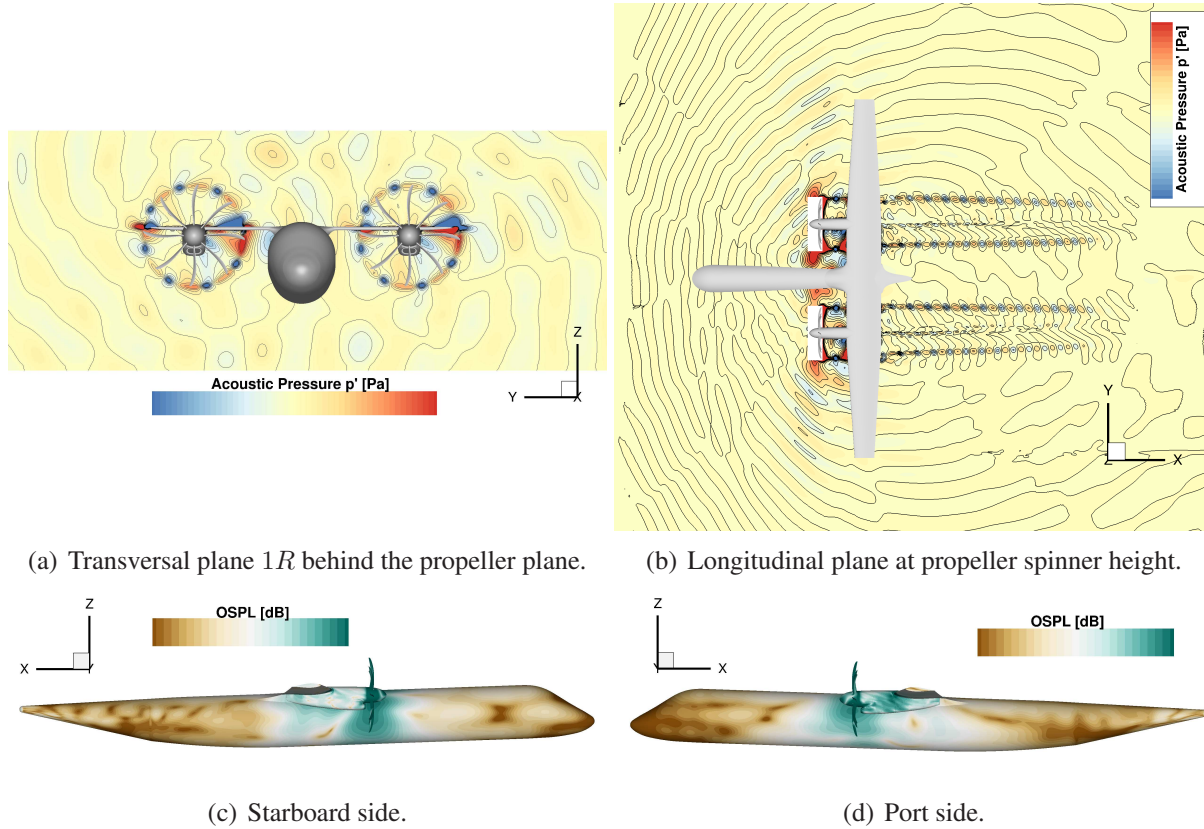
(c) Starboard side.

(d) Port side.

Figure 2: Sound field for the co-rotating layout with propellers in phase: instantaneous unsteady pressure field visualisation ($\psi_b = 90$ deg) at the top and OSPL on the aircraft external surface (estimate from URANS results over a quarter of propeller revolution - color scale range equal to 45 dB) at the bottom.

Port and starboard sides display marked differences for co-rotating propellers, with a slight change in the azimuthal position and extent of the main noise lobes depending on the blade shift in phase. In contrast, the acoustic field and the noise distribution on the aircraft are symmetric in the case of counter-rotating propellers (with no synchrophasing). Small differences in the OSPL are also seen for the same propeller rotational direction but for different installation options (i.e. looking at the aircraft port side of phased co-rotating propellers and counter-rotating top-in layout or at the starboard side of phased co-rotating propellers and counter-rotating top-out layout), indicating the importance of the interaction of the acoustic fields of the two propellers and the ability of the CFD method to solve it.

To better evaluate, quantitatively, the various cases considered, the area of higher noise levels, i.e. from around 1 radius ahead of the propeller plane up to the wing-fuselage junction, was analysed using the data from numerical probes included in the simulations. Figures 3(a) and 3(c) present, as an example, the OSPL at the propeller plane as a function of the fuselage azimuthal position. Figure 3(a) compares co-rotating in phase, counter-rotating top-in and counter-rotating top-out layouts, and results of the isolated case in axial flight are reported as reference. As can
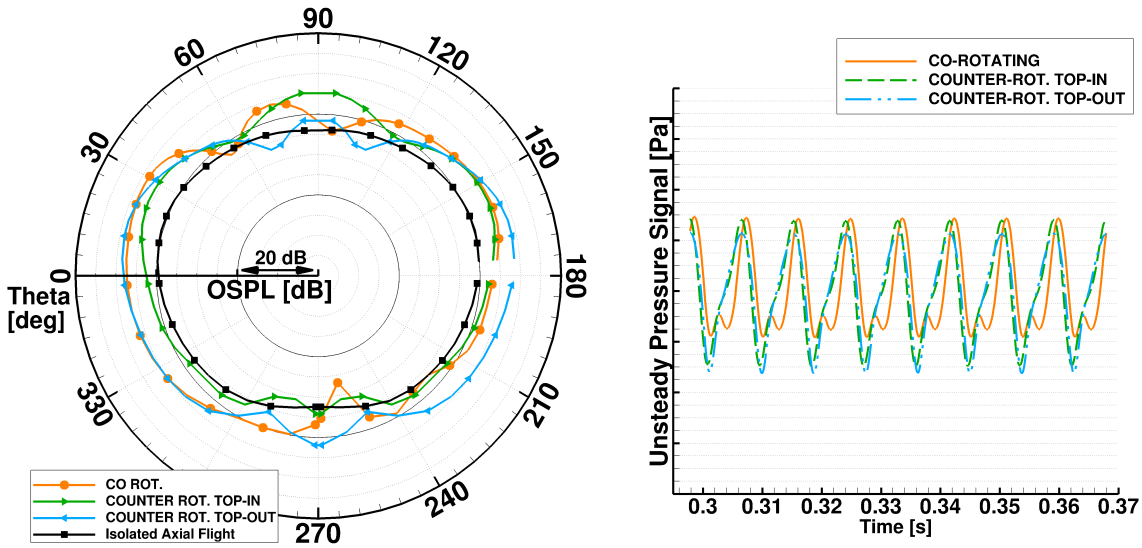
(a) OSPL distribution as function of the fuselage azimuth θ at the propeller plane: comparison between co-rotating and counter-rotating layouts as well as the isolated propeller in axial flight.

(b) Unsteady pressure waveforms, for one propeller revolution, on the aircraft fuselage at the propeller plane, at $\theta = 57$ deg: comparison between co-rotating and counter-rotating layouts.
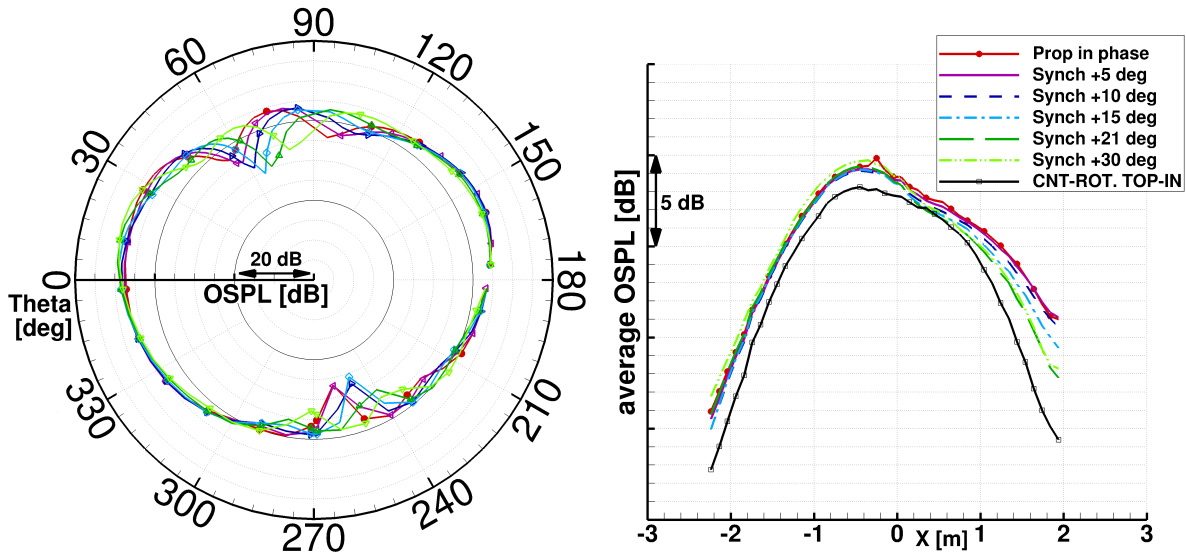
(c) OSPL distribution as function of the fuselage azimuth θ at the propeller plane: comparison between co-rotating phased propellers and synchrophasing cases. Refer to Figure 3(d) for the colour legend.

(d) OSPL averaged over the fuselage azimuth θ, in the passengers area, as a function of the fuselage longitudinal position: comparison between co-rotating cases and counter-rotating top-in scenario as a reference.

Figure 3: Fuselage exterior noise evaluation: comparison between the different propeller installation options. Noise estimate from numerical probes data over one full propeller revolution.

be seen, the differences between isolated and installed propeller cases are substantial, regarding both noise levels and pattern, making the cheap single-blade steady simulation not suitable to evaluate the actual sound on the flying aircraft. The local OSPL reductions predicted for the installed cases towards the top and the bottom of the fuselage are the result of interferences occurring between sound waves of the various sound sources. Looking at the unsteady pressure waveforms recorded by the probes at these locations (see for example Figure 3(b)) it is possible to distinguish a second frequency in addition to the predominant eight-period oscillation related to the blade passage. Differences, among co-rotating and counter-rotating configurations, in the amplitude of the pressure perturbations and their phase are also evident and can lead to OSPL discrepancies up to 5 or 6 dB for certain azimuthal locations. As anticipated from the acoustic field analysis, the inboard-up propeller direction yields higher sound levels than the inboard-down. The OSPL distribution in the case of co-rotating propellers is very close, even though some differences are visible, to the one of the counter-rotating top-out propellers on the starboard side and to the one of the counter-rotating top-in propellers on the port side in the central part of the fuselage. Large differences are instead noted near the top area of the fuselage, where the sound waves from the two propellers interfere, creating a different acoustic field depending on the installation option. In general, the main effect of the positive synchrophase angle (see Figure 3(c)) appears to be a shift of the noise upper lobe towards slightly larger fuselage azimuthal angles. Differences in the sound levels of the noise maxima are at most 2 dB, whereas larger differences are seen regarding the points of minimum noise, where synchrophasing show reductions of up to 5 dB more than phased propellers, indicating a stronger destructive interference between acoustic sources.

Regions up-stream of the propeller rotational plane, and up to one propeller radius behind it show very similar OSPL azimuthal distributions, with decreasing noise levels when increasing the distance from the propeller plane. Further aft, where the sound emanating by the interactions with the airframe also affects the OSPL on the fuselage, the azimuthal noise distribution is more irregular and the differences between the various test cases become larger and substantial (up to 10 dB of difference are visible for some azimuthal locations around $R/2$ away from the propeller plane). A couple of additional upper-lateral lobes is noticed, whose peak noise levels vary with the fuselage station and decrease with a positive increase of the synchrophase angle. It is interesting that the counter-rotating top-in layout is the only one showing, at equal distances from the propeller plane, lower OSPL values down-stream than up-stream.

Globally, the counter-rotating top-in option appears the quietest, as it can be also seen in Figure 3(d) where the azimuthally-averaged OSPL value is presented as function of the fuselage longitudinal axis. Synchrophasing has a beneficial effect behind the propeller plane, specially closer to the wing-fuselage junction, indicating that propeller synchrophasing modifies not only the acoustic interference that develops between the sound fields of the two propellers, but also, and in greater ways, the interference of the propeller's direct sound fields with the one produced from the interactions with the airframe. Larger synchrophase angles provide larger noise reductions in this area, with a non-linear relation between ψ_s and OSPL, the maximum achieved for $\psi_s \leq 21$ deg. However, ahead of the propeller plane, where differences are smaller, larger synchrophase angles may yield increased in sound levels. Anyhow, at these flight conditions, noise gains achieved by synchrophasing appear smaller, at all fuselage stations, than that provided by

the choice of a counter-rotating top-in layout.

4.2 Cabin Interior Noise

The SPL for the first three propeller harmonics and the OSPL of the sound signal that would be heard by the passenger example are presented, for all test cases, in Figure 4 and Table 2. Co-rotating in phase propellers are shown to be the loudest option at this flight condition, and the counter-rotating top-in configuration the quietest. The latter exhibits significant noise reductions at the three first tones, yielding an OSPL decrease of more than 4 dB. Synchrophasing is also observed to have a considerable beneficial effect regarding cabin noise.
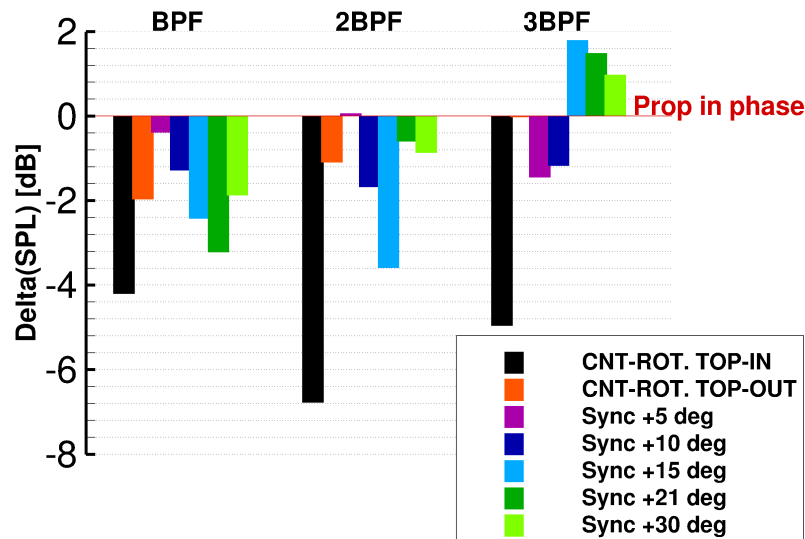

Figure 4: Cabin interior sound evaluation, for the example passenger, using experimental TF: comparison of the SPL for first, second and third tone between the different propeller installation options. Relative data with respect to the case with co-rotating phased propellers.

Table 2: Cabin interior sound evaluation, for the example passenger, using experimental TF: comparison of the OSPL between the different propeller installation options. Relative data with respect to the case with co-rotating phased propellers

CNTI Layout	-4.21 dB
CNTO Layout	-1.97 dB
$\psi_s = 5$ deg	-0.39 dB
$\psi_s = 10$ de	-1.29 dB
$\psi_s = 15$ deg	-2.42 dB
$\psi_s = 21$ deg	-3.21 dB
$\psi_s = 30$ deg	-1.87 dB

10

The choice of $\psi_s = 21$ deg appears the best among the angles considered, providing a noise gain of more than 3 dB, mainly thanks to the reduction of the first harmonic SPL. Smaller angles are less effective, while larger angles are not ideal because of the sound levels increase registered ahead of the propeller plane. It is finally interesting to note that even the counter-rotating top-out layout, which has both propellers rotating inboard-up, shows lower noise levels than co-rotating phased propellers. This suggests the development of some destructive interferences in the counter-rotating case between the sound fields of the two propellers that do not occur in the co-rotating case (the pressure disturbance that travels ahead form the fuselage surface at the height of the propeller plane is also seen to be smaller in the external acoustic field visualisations).

5 CONCLUSIONS

URANS computations of a full twin-engined turboprop aircraft were successfully carried out with the HMB3 flow solver to investigate propellers installation effects on the near-field aircraft acoustics and cabin noise. The eight-bladed IMPACTA propeller, representative of a modern propeller design, was employed. Co-rotating propellers, in phase as well as with synchrophasing, and counter-rotating propellers were considered. Significant differences were observed in the exterior acoustic field between co-rotating and counter-rotating configurations whereas, in line with previous studies, synchrophasing is shown to mainly affect the interior noise. At the cruise conditions tested, the counter-rotating top-in option appears the quietest, with a benefit of more than 4 dB for the example passenger compared to co-rotating phased propellers. The inboard-up propeller rotation yields to louder noise because of the higher blade loading on the inboard propeller side and because of constructive acoustic interferences between direct propeller sound waves and noise emitted, as well as reflected, from the interactions with the airframe. However, in the case of counter-rotating top-out layout some destructive interferences occur and also this option, which displays the highest aerodynamic efficiency, shows a OSPL reduction at the example passenger location of almost 2 dB with respect to co-rotating phased propellers. More than 3 dB of OSPL gain can instead be achieved with synchrophasing, with the best angle tested being $\psi_s = 21$ deg, i.e. close to the maximum relative blade shift angle. The noise reduction obtained via synchrophasing appears mainly between the propeller plane and the wing, indicating the existence of favorable acoustic interferences that develop between the propellers direct sound field and the waves emanating by the airframe.

Future Work Further developments of this study should assess the effectiveness of synchrophasing for the counter-rotating top-in layout to see if larger noise gains can be achieved by adding the two beneficial effects. Moreover, a different blade design proven considerably quieter in isolation[47] should be analysed installed on the aircraft to evaluate how much it can contribute to the noise reduction achieved by the choice of the installation layout.

Acknowledgements

NOMENCLATURE

Acronyms

BPF Blade Passing Frequency

CFD Computation Fluid Dynamics

OSPL Overall SPL

SPL Sound Pressure Level

TF Transfer Function

URANS Unsteady Reynold Averaged Navier-Stokes

Greek Symbols

Θ Fuselage azimuthal coordinate [deg]

ψ_b Azimuthal position of reference blade [deg]

ψ_s Starboard propeller synchrophase angle [deg]

Latin Symbols

$p'(\mathbf{x}, t)$ Unsteady pressure time signal [Pa]

R Propeller Radius [m]

X Fuselage longitudinal coordinate [m]

References

[1] Pedro Argüelles, Manfred Bischoff, Philippe Busquin, BAC Droste, Sir Richard Evans, W Kröll, JL Lagardere, A Lina, J Lumsden, D Ranque, et al. European Aeronautics: a Vision for 2020 - Meeting Society's Needs and Winning Global Leadership. Technical report, European Commission, Directorate General for Research and Innovation - Advisory Council for Aeronautics Research in Europe, 2001. URL http://www.acare4europe.org/sites/acare4europe.org/files/document/Vision%202020_0.pdf.

[2] The High Level Group on Aviation Research: M. Darecki, C. Edelstenne, T. Enders, E. Fernandez, P. Hartman, J.-P. Herteman, M. Kerkloh, I. King, P. Ky, M. Mathieu, G. Orsi, G. Schotman, C. Smith, and J.-D. Wörner. Flightpath 2050: Europe's vision for aviation. report of the high level group on aviation research. Technical report, ACARE (Advisory Council for Aeronautics Research in Europe) - Publications Office of the European Union, Luxembourg, 2011. URL http://ec.europa.eu/transport/sites/transport/files/modes/air/doc/flightpath2050.pdf.

[3] R.P. Woodward and I.J. Loeffler. In-flight source noise of an advanced large-scale single-rotation propeller. *Journal of Aircraft*, 30(6):918–926, 1993. doi: 10.2514/3.46435. URL https://doi.org/10.2514/3.46435.

[4] R.P. Woodward and I.J. Loeffler. In-flight near-and far-field acoustic data measured on the Propfan Test Assessment (PTA) testbed and with an adjacent aircraft. Technical Report NASA-TM-103719, E-6402, NAS 1.15:103719, NASA Lewis Research Center; Cleveland, OH, United States, April 1993. URL https://ntrs.nasa.gov/archive/nasa/casi.ntrs.nasa.gov/19930017869.pdf.

[5] M.H. Dunn and G.M. Tarkenton. Computational methods in the prediction of advanced subsonic and supersonic propeller induced noise: ASSPIN users' manual. Technical Report NASA-CR-4434, NAS 1.26:4434, NASA. Langley Research Center, Washington, United States, 1992. URL https://ntrs.nasa.gov/search.jsp?R=19920012215.

[6] D.B. Hanson. Near-field frequency-domain theory for propeller noise. *AIAA journal*, 23(4):499–504, 1985. doi: 10.2514/3.8943. URL https://doi.org/10.2514/3.8943.

[7] E Envia. Prediction of noise field of a propfan at angle of attack. Technical Report NASA-CR-189047, E-6645, NAS 1.26:189047, NASA, United States, October 1991. URL https://ntrs.nasa.gov/archive/nasa/casi.ntrs.nasa.gov/19920004541.pdf.

[8] M. Nallasamy and F. Groeneweg. Unsteady euler analysis of the flowfield of a propfan at an angle of attack. *Journal of Propulsion and Power*, 8(1):136–143, 1992. doi: 10.2514/3.23453. URL https://doi.org/10.2514/3.23453.

[9] A. Dumas and C. Castan. Aerodynamic Integration of High Speed Propeller on Aircraft Recent Investigations in European Wind Tunnels. In *21st ICAS Congress, Melbourne (Australia)*, pages 1–11. International Council of the Aeronautical Sciences, 1998. ISBN ISBN-10: 1-56347-287-2, ISBN-13: 978-1-56347-287-9. URL

http://www.icas.org/ICAS_ARCHIVE/ICAS1998/PAPERS/5103.PDF. Paper ICAS-98-5.10.3.

[10] M. Amato, F. Boyle, J. Eaton, and P. Gardarein. Euler/Navier-Stokes simulation for propulsion airframe integration of advanced propeller-driven aircraft in the European Research Programs GEMINI/APIAN. In *21st ICAS Congress, Melbourne (Australia)*, pages 1–12. International Council of the Aeronautical Sciences, 1998. ISBN ISBN-10: 1-56347-287-2, ISBN-13: 978-1-56347-287-9. URL http://www.icas.org/ICAS_ARCHIVE/ICAS1998/PAPERS/5102.PDF. Paper ICAS 98-5.10.2.

[11] J.M. Bousquet and P. Gardarein. Improvements on computations of high speed propeller unsteady aerodynamics. *Aerospace science and technology*, 7(6):465–472, 2003. ISSN 1270-9638. doi: https://doi.org/10.1016/S1270-9638(03)00046-4. URL http://www.sciencedirect.com/science/article/pii/S1270963803000464.

[12] J. Frota and E. Maury. Analysis of APIAN high speed isolated test results - Acoustics and Aerodynamics. *Air and Space Europe*, 3(3):87–92, 2001. ISSN 1290-0958. doi: https://doi.org/10.1016/S1290-0958(01)90064-4. URL http://www.sciencedirect.com/science/article/pii/S1290095801900644.

[13] C. Polacsek, P. Spiegel, F. Boyle, J. Eaton, H. Brouwer, and R. Nijboer. Noise computation of high-speed propeller-driven aircraft. In *6th Aeroacoustics Conference and Exhibit*. American Institute of Aeronautics and Astronautics, 2000. doi: 10.2514/6.2000-2086. URL https://doi.org/10.2514/6.2000-2086. Paper AIAA-2000-2086.

[14] I. Samuelsson. Low speed wind tunnel investigation of propeller slipstream aerodynamic effects on different nacelle/wing combinations. In *ICAS, Congress, 16 th, Jerusalem (Israel)*, pages 1749–1765. International Council of the Aeronautical Sciences, 1988. URL http://www.icas.org/ICAS_ARCHIVE/ICAS1988/ICAS-88-4.11.1.pdf. Paper ICAS-88-4.11.1.

[15] I. Samuelsson. Experimental investigation of low speed model propeller slipstream aerodynamic characteristics including flow field surveys and nacelle/wing static pressure measurements. In *ICAS, Congress, 17 th, Stockholm (Sweden)*, pages 71–84. International Council of the Aeronautical Sciences, 1990. URL http://www.icas.org/ICAS_ARCHIVE/ICAS1990/ICAS-90-3.1.3.pdf. Paper ICAS-90-3.1.3.

[16] P. Lotsted. Propeller slip-stream model in subsonic linearized potential flow. *Journal of Aircraft*, 29 (6):1098–1105, 1992. doi: 10.2514/3.56865. URL https://doi.org/10.2514/3.56865.

[17] P. Lotsted. A propeller slipstream model in subsonic linearized potential flow. In *ICAS, Congress, 17 th, Stockholm (Sweden)*, pages 733–744. International Council of the Aeronautical Sciences, 1990. URL http://www.icas.org/ICAS_ARCHIVE/ICAS1990/ICAS-90-5.4.4.pdf. Paper ICAS-90-5.4.4.

[18] S. Leth, F. Samuelsson, and S. Meijer. Propeller Noise Generation and its Reduction on the Saab 2000 High-Speed Turboprop. In *4th AIAA/CEAS Aeroacoustics Conference*, pages 457–463. American Institute of Aeronautics and Astronautics, 1998. doi: 10.2514/6.1998-2283. URL `https://doi.org/10.2514/6.1998-2283`. Paper AIAA-98-2283.

[19] Urban Emborg, Fredrik Samuelsson, Joakim Holmgren, and Siv Leth. Active and passive noise control in practice on the saab 2000 high speed turboprop. In *4th AIAA/CEAS aeroacoustics conference*, pages 1–5. American Institute of Aeronautics and Astronautics, 1998. doi: 10.2514/6.1998-2231. URL `https://doi.org/10.2514/6.1998-2231`.

[20] R.A. Akkermans, M. Pott-Pollenske, H. Buchholz, J. Delfs, D. Almoneit, et al. Installation Effects of a Propeller Mounted on a High-Lift Wing with a Coanda Flap. Part I: Aeroacoustic Experiments. In *20th AIAA/CEAS Aeroacoustics Conference - AIAA AVIATION Forum*, pages 1–14. American Institute of Aeronautics and Astronautics, 2014. doi: 10.2514/6.2014-3191. URL `https://doi.org/10.2514/6.2014-3191`. Paper AIAA 2014-3191.

[21] C. Lenfers, N. Beck, and R. Radespiel. Numerical and experimental investigation of propeller slipstream interaction with active high lift wing. In *35th AIAA Applied Aerodynamics Conference - AIAA AVIATION Forum*, pages 1–14. American Institute of Aeronautics and Astronautics, 2017. doi: 10.2514/6.2017-3248. URL `https://arc.aiaa.org/doi/pdf/10.2514/6.2017-3248`.

[22] J. Yin, A. Stuermer, and M. Aversano. Aerodynamic and aeroacoustic analysis of installed pusher-propeller aircraft configurations. *Journal of Aircraft*, 49(5):1423–1433, 2012. doi: 10.2514/1.C031704. URL `https://doi.org/10.2514/1.C031704`.

[23] A. Pagano, M. Barbarino, D. Casalino, and L. Federico. Tonal and Broadband Noise Calculations for Aeoacoustic Optimization of a Pusher Propeller. *Journal of Aircraft*, 47(3):835–848, 2010. doi: 10.2514/1.45315. URL `https://doi.org/10.2514/1.45315`.

[24] C.R. Fuller. Noise control characteristics of synchrophasing. I-Analytical investigation. *AIAA journal*, 24(7):1063–1068, 1986. doi: 10.2514/3.9392. URL `https://doi.org/10.2514/3.9392`.

[25] J.D. Jones and C.R. Fuller. Noise control characteristics of synchrophasing. II-Experimental investigation. *AIAA journal*, 24(8):1271–1276, 1986. doi: 10.2514/3.9431. URL `http://dx.doi.org/10.2514/3.9431`.

[26] J.F. Johnston, R.E. Donham, and W.A. Guinn. Propeller signatures and their use. *Journal of Aircraft*, 18(11):934–942, 1981. doi: http://dx.doi.org/10.2514/3.57583.

[27] B. Magliozzi. Synchrophasing for cabin noise reduction of propeller-driven airplanes. In *8th Aeroacoustics Conference*, pages 1–7. American Institute of Aeronautics and Astronautics, 1983. doi: 10.2514/6.1983-717. URL `https://doi.org/10.2514/6.1983-717`. Paper AIAA-83-0717.

[28] D.M. Blunt. Altitude and airspeed effects on the optimum synchrophase angles for a four-engine propeller aircraft. *Journal of Sound and Vibration*, 333(16):3732–3742, 2014. ISSN 0022-460X. doi: https://doi.org/10.1016/j.jsv.2014.03.038. URL `http://www.sciencedirect.com/science/article/pii/S0022460X14002399`.

[29] D. Hammond, R. McKinley, and B. Hale. Noise reduction efforts for special operations c-130 aircraft using active synchrophaser control. Technical report, Air Force Rsearch Lab,Wright Patterson AFB,OH,45433, 1998. URL http://www.dtic.mil/dtic/tr/fulltext/u2/a434029.pdf.

[30] F.G. Pla and G.C. Goodman. Method and apparatus for synchronizing rotating machinery to reduce noise, June 1993. URL https://www.google.com/patents/US5221185. US Patent 5221185.

[31] F.G. Pla. Method for reducing noise and/or vibration from multiple rotating machines, August 1998. URL https://www.google.com/patents/US5789678. US Patent 5789678.

[32] D. Kaptein. Propeller blade position controller, September 1996. URL https://www.google.com/patents/US5551649. US Patent 5551649, DE69526464D1, EP0663337B1.

[33] B. Magliozzi. Adaptive synchrophaser for reducing aircraft cabin noise and vibration, September 1995. URL https://patents.google.com/patent/WO1995022488A1/en. US Patent 5453943, WO1995022488A1.

[34] L.J. Eriksson. Active sound attenuation system with on-line adaptive feedback cancellation, June 1987. US Patent 4677677, CA1282161C.

[35] D.M. Blunt and B. Rebbechi. Propeller synchrophase angle optimisation study. In *13th AIAA/CEAS Aeroacoustics Conference (28th AIAA Aeroacoustics Conference)*, page 3584. American Institute of Aeronautics and Astronautics, 2007. doi: 10.2514/6.2007-3584. URL https://doi.org/10.2514/6.2007-3584. Paper AIAA 2007-3584.

[36] X. Huang, L. Sheng, and Y. Wang. Propeller synchrophase angle optimization of turboprop-driven aircraft—an experimental investigation. *Journal of Engineering for Gas Turbines and Power*, 136(11):112606–1–112606–9, 2014. doi: 10.1115/1.4027644. URL http://dx.doi.org/10.1115/1.4027644.

[37] G.N. Barakos, R. Steijl, K. Badcock, and A. Brocklehurst. Development of CFD Capability for Full Helicopter Engineering Analysis. In *31st European Rotorcraft Forum, Florence (Italy)*, pages 1–15, 2005. ISBN 9781617389566.

[38] R. Steijl, G. Barakos, and K. Badcock. A Framework for CFD Analysis of Helicopter Rotors in Hover and Forward Flight. *International Journal for Numerical Methods in Fluids*, 51(8):819–847, 2006. ISSN 1097-0363. doi: 10.1002/fld.1086. URL http://dx.doi.org/10.1002/fld.1086.

[39] S.J. Lawson, M. Woodgate, R. Steijl, and G.N. Barakos. High Performance Computing for Challenging Problems in Computational Fluid Dynamics. *Progress in Aerospace Sciences*, 52: 19–29, July 2012. ISSN 0376-0421. doi: https://doi.org/10.1016/j.paerosci.2012.03.004. URL http://www.sciencedirect.com/science/article/pii/S0376042112000371. Applied Computational Aerodynamics and High Performance Computing in the UK.

[40] S. Osher and S. Chakravarthy. Upwind Schemes and Boundary Conditions with Applications to Euler Equations in General Geometries. *Journal of Computational Physics*, 50(3): 447–481, 1983. ISSN 0021-9991. doi: https://doi.org/10.1016/0021-9991(83)90106-7. URL `http://www.sciencedirect.com/science/article/pii/0021999183901067`.

[41] J. Boussinesq. *Théorie de l'Écoulement Tourbillonant et Tumultueux des Liquides dans des Lits Rectilignes à Grande Section, Tome I-II (Theory of the swirling and turbulent flow of liquids in straight channels of large section, Volume I-II)*. Gaulthier-Villars, Paris, France, first edition, 1897.

[42] A.K. Hellsten. New advanced kw turbulence model for high-lift aerodynamics. *AIAA journal*, 43 (9):1857–1869, 2005. doi: 10.2514/1.13754. URL `https://doi.org/10.2514/1.13754`.

[43] B. van Leer. Flux-vector Splitting for the Euler Equations. In *Eighth International Conference on Numerical Methods in Fluid Dynamics*, pages 507–512. Springer Berlin Heidelberg, 1997. ISBN 978-3-540-39532-4. doi: 10.1007/978-3-642-60543-7_5.

[44] G.D. van Albada, B. van Leer, and W.W. Roberts Jr. A Comparative Study of Computational Methods in Cosmic Gas Dynamics. In *Upwind and High-Resolution Schemes*, volume 2, pages 95–103. Springer Berlin Heidelberg, 1997. ISBN 978-3-642-60543-7. doi: 10.1007/978-3-642-60543-7_6. URL `https://doi.org/10.1007/978-3-642-60543-7_6`.

[45] O. Axelsson. *Iterative Solution Methods*. Cambridge University Press, Cambridge, MA, 1994. ISBN 9780511624100. doi: 10.1017/CBO9780511624100. URL `https://doi.org/10.1017/CBO9780511624100`.

[46] G.N. Barakos and C.S. Johnson. Acoustic comparison of propellers. *International Journal of Aeroacoustics*, 15(6-7):575–594, 2016. doi: 10.1177/1475472X16659214. URL `https://doi.org/10.1177/1475472X16659214`.

[47] G. Chirico, G.N. Barakos, and N. Bown. Numerical aeroacoustic analysis of propeller designs. *The Aeronautical Journal*, 122(1248):283–315, 2018. doi: 10.1017/aer.2017.123. URL `https://doi.org/10.1017/aer.2017.123`.

[48] E.G.M. Geurts. IMPACTA Transmission functions generation - test and processing. Technical Report NLR-CR-2013-145, National Aerospace Laboratory NLR, 2013.

[49] G. Chirico, G.N. Barakos, and N. Bown. Propeller Installation Effects on Turboprop Acoustics. Part I: Co-rotating *vs* Counter-rotating Layouts. *Journal of Sound and Vibration*, - Under review, 2018.

[50] G. Chirico, G.N. Barakos, and N. Bown. Propeller Installation Effects on Turboprop Acoustics. Part II: CFD Assessing of Synchrophasing. *Journal of Sound and Vibration*, - Under review, 2018.

[51] F.R. Menter. Two-Equation Eddy-Viscosity Turbulence Models for Engineering Applications. *AIAA Journal*, 32(8):1598–1605, August 1994. doi: 10.2514/3.12149. URL `https://doi.org/10.2514/3.12149`.

[52] R. Steijl and G. Barakos. Sliding Mesh Algorithm for CFD Analysis of Helicopter Rotor˘Fuselage Aerodynamics. *International Journal for Numerical Methods in Fluids*, 58(5):527–549, 2008. ISSN 1097-0363. doi: 10.1002/fld.1757. URL `http://dx.doi.org/10.1002/fld.1757`.

[53] M. Jarwowsky, M.A. Woodgate, G. Barakos, and J. Rokicki. Towards Consistent Hybrid Overset Mesh Methods for Rotorcraft CFD. *International Journal for Numerical Methods in Fluids*, 74(8):543–576, 2014. ISSN 1097-0363. doi: 10.1002/fld.3861. URL http://dx.doi.org/10.1002/fld.3861.

[54] Dowty Aerospace Propellers. URL http://dowty.com. (Accessed 23 February 2018).